Variation of charge-ordering transitions in $R_{1/3}Sr_{2/3}FeO_3$ ($R=$La, Pr, Nd, Sm, and Gd)

S. K. Park,* T. Ishikawa,† and Y. Tokura

Department of Applied Physics, University of Tokyo, Tokyo 113-8656, Japan

J. Q. Li‡ and Y. Matsui

National Institute for Research in Inorganic Materials, 1-1 Namiki, Tsukuba, Ibaraki 305-0044, Japan

The change of the electronic and magnetic properties as well as the charge-ordering (CO) transition related with lattice dynamics has been systematically investigated for crystals of $R_{1/3}Sr_{2/3}FeO_3$ ($R=$La, Pr, Nd, Sm, and Gd) by transmission electron microscopy and measurements of transport, magnetic, and optical properties. In $R_{1/3}Sr_{2/3}FeO_3$, the hybridization of O $2p$ and Fe $3d$ states, or the effective d electron hopping interaction, can be controlled to some extent by R-dependent lattice distortion. The $La_{1/3}Sr_{2/3}FeO_3$ with least rhombohedral lattice distortion undergoes a CO phase transition with $T_{CO}=198$ K accompanying charge disproportionation into nominally Fe^{3+} and Fe^{5+} sites, as well as antiferromagnetic spin ordering. When the R-site ion is changed from $R=$La to smaller-size R ion towards $R=$Gd, and hence the p-d hybridization interaction is decreased, T_{CO} is decreased and finally the CO transition disappears for $R=$Sm and Gd. The optical conductivity spectra for the $R=$La – Nd compounds show a gap opening below T_{CO} and several activated phonon modes due to the periodic charge modulation. The spectral intensity of the new phonon modes shows a discontinuous increase at T_{CO} reflecting the first-order nature of the CO transition. In the cases of the $R=$Sm and Gd compounds with no CO transition, the gap feature is observed over a whole temperature region, while no phonon anomaly is discerned. These results imply that the strong p-d hybridization as realized for $R=$La, Pr, and Nd is necessary for stabilizing the specific valence-skipping charge-ordered state. [S0163-1829(99)03039-8]

I. INTRODUCTION

The study on transition-metal oxides (TMO's) with strong electron correlation has been unraveling many intrigue phenomena,[1] for example, high T_C superconductivity in cuprate and colossal magnetoresistance in manganites. Order-disorder phenomena of charge, spin, and orbital in TMO's are important issues in the light of metal-insulator transitions. Among them, charge-ordering/disordering transitions are a long-standing problem but also of current great interest. The charge-ordering (CO) transition is seen in many TMO's; for example, Verwey transition in Fe_3O_4 with spinel structure,[2] x (hole doping)=1/8 anomaly of the high T_C-superconducting cuprates,[3] colossal magnetoresistive manganites ($x\approx1/2$),[4,5] layered nickelates ($x\approx1/3$),[6,7] layered manganites ($x\approx1/2$),[8] and so on. The perovskite-type $La_{1-x}Sr_xFeO_3$ is one such example. The end compound of this system $LaFeO_3$ ($x=0$) is a charge-transfer type insulator with a charge gap of about 2 eV due to the strong on-site coulomb repulsion.[9] The valence of the Fe ion, or the nominal hole doping level, in this system can be varied from $+3$ ($3d^5$, $x=0$) to $+4$ ($3d^4$, $x=1$) by substitution of trivalent La ions with divalent Sr ions. The hole doping greatly reduces the value of resistivity, although the compound remains insulating at low temperatures, at least up to $x\approx0.7$. One of the origins of the insulating ground state of the moderately hole-doped compound is the CO, which shows up most conspicuously around $x=2/3$ in $La_{1-x}Sr_xFeO_3$.[10]

A pioneering research on this phenomenon was carried out by Takano *et al.*[11] with use of Mössbauer spectroscopy. The charge disproportionation was detected at low temperatures below 200 K, in which two kinds of Fe ions with va-

lence states of $+3$ (Fe^{3+}) and $+5$ (Fe^{5+}) were found with the ratio of 2:1. Such an anomalous valence state as well as the real space ordering of valence-skipping sites was observed also by measurements of magnetic neutron scattering,[12] which indicated that the ordered layers of Fe^{3+} and Fe^{5+} ions are in the sequences of ...335335... along the rhombohedral z direction or the pseudocubic-perovskite $[111]_c$ direction. More lately, such a CO state was verified by transmission electron microscopy[13] (TEM) which probed the presence of structural modulation related to the charge-ordered state. In this paper, we report on variation of such a CO transition in $R_{1/3}Sr_{2/3}FeO_3$ with varying R site (La, Pr, Nd, Sm, and Gd) or equivalently with varying the magnitude of p-d hybridization.

Modification of chemical composition on the perovskite A site is effective for controlling fundamental electronic parameters, such as electron hopping interaction and doping level, in perovskite-type TMO's.[1] In the case of $R_{1-x}Sr_xFeO_3$, it is possible to control the hybridization (t_{pd}) between Fe $3d$ and O $2p$ states or the one-electron bandwidth (W) of the conduction electron band by changing the average ionic radius of the perovskite A site (R, Sr) while keeping the doping level fixed at $x=2/3$. When the R-site ion on the A site is changed from La to Gd (namely, decreasing the ionic radius), the distortion of FeO_6-octahedral structure is increased to decrease the bond angle ($\angle$ Fe-O-Fe) from 180° in an ideal cubic perovskite structure. Therefore, the hybridization between oxygen $2p$ σ and Fe $3d$ e_g states is weakened and accordingly electron transfer interaction is decreased or the W is narrowed. Intuitively, the long-range Coulomb interaction, which should compete with W might
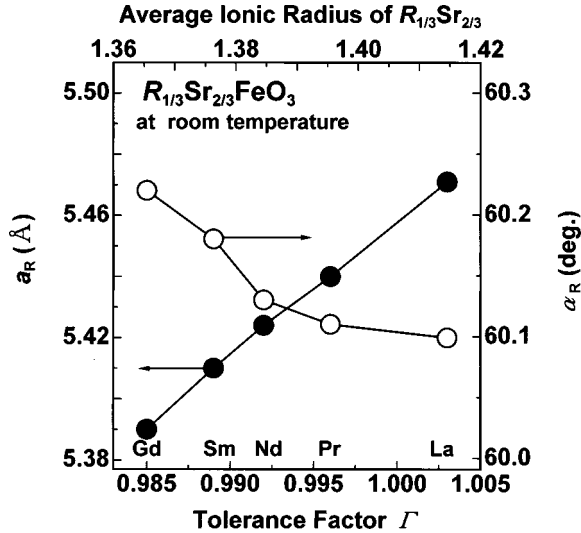
FIG. 1. R dependence of the lattice parameters for $R_{1/3}Sr_{2/3}FeO_3$ (R=La, Pr, Nd, Sm, and Gd) system at room temperature.

favor the charge-ordered state in the small-R system, whereas we may have to consider the anomalous high-valence nature of Fe^{5+} state that should be stabilized by strong d-p hybridization, which causes O $2p$-hole character. To clarify such a complicated but interesting effect of the t_{pd} or W on the CO transition is one of motivations of the present systematic study on $R_{1/3}Sr_{2/3}FeO_3$ with varying R (=La, Pr, Nd, Sm, and Gd). We have investigated the change of the electronic and magnetic structure as well as the lattice structure and dynamics in the $R_{1/3}Sr_{2/3}FeO_3$ system by measurements of transmission electron microscopy, and transport, magnetic, and optical properties.

II. EXPERIMENT

A. Sample preparation and characterization

All samples used in the present paper were obtained using the floating-zone method. Starting materials were R_2O_3 (R =La, Pr, Nd, Sm, and Gd), $SrCO_3$, and α-Fe_2O_3 which was well dried at $900\,°C$ for 5 h. A stoichiometric mixture of respective materials with a prescribed ratio for $R_{1/3}Sr_{2/3}FeO_3$ was ground for 1 h in an automatic ball mill and calcined at $1100\,°C$ for 20 h in air, and the process was repeated three times. Then the resulting powder was pressed into a feed rod with a size of 5 $mm\phi \times 100$ mm and sintered in oxygen gas at $1260 - 1310\,°C$ for 50 h. The apparatus used for the crystal growth was the floating-zone furnace equipped with two halogen incandescent lamps and hemielliptic focusing mirrors. The feed and seed rods were rotated in opposite directions at a relative rate of 20 rpm and the feeding speed of crystal wes kept at 1.0 mm/h for all the samples. The atmosphere during the crystal growth was about 6 atm of oxygen for all the samples. Homogeneity of the composition was confirmed by electron probe microanalysis. The crystal structure was characterized by x-ray powder diffraction with Cu $K\alpha$ radiation, which indicated that all the samples were single phase and exhibited distorted perovskite structure with rhombohedral ($R\bar{3}c$) form.

In Fig. 1, we show a variation of the lattice parameters of

$R_{1/3}Sr_{2/3}FeO_3$ crystals with R ion at room temperature. The decrease of the average ionic radius of the (R, Sr) site leads to the decrease of the lattice constant (a_R) from 5.47 Å (R=La) to 5.39 Å (R=Gd) and to the increase of the edge angle (α_R) from $60.10°$ (R=La) to $60.22°$ (R=Gd), namely the increase of the rhombohedral lattice distortion. We use the tolerance factor[14] (Γ) as a measure of the lattice distortion instead of the detailed crystal lattice parameters, defined as

$$\Gamma = \frac{\langle r_{R,Sr}\rangle + r_O}{\sqrt{2}(r_{Fe} + r_O)}. \tag{1}$$

Here, $\langle r_{R,Sr}\rangle$, r_{Fe}, and r_O are the average ionic radii of the (R, Sr) site, Fe, and O, respectively. When Γ is closer to 1, the crystal lattice should be, by definition, closer to the ideal cubic structure. When the R-site ion changes from La to Gd, the value of Γ for $R_{1/3}Sr_{2/3}FeO_3$ is changed from 1.003 (La) to 0.985 (Gd), as indicated on the lower abscissa of Fig. 1.

B. Transmission electron microscopy and measurements of transport, magnetic, and optical properties

For measurements of the TEM, the samples were pulverized together with CCl_4 and dispersed on Cu grids coated with holy-carbon support files using an apparatus of Hitachi H-1500 high-resolution microscope operated at 800 kV. Resistivity measurements (5–300 K) were performed on the specimen of a rectangular shape (typically $1.5 \times 1.0 \times 0.5$ mm^3) by the conventional four-probe technique using heat-treatment-type silver paint as an electrode. Magnetic measurements (3–300 K) were performed using a superconducting quantum interference device magnetometer. For optical measurements a disk was sliced out from the crystal baule and polished to a mirrorlike surface with alumina powder. The near-normal incidence reflectivity spectra were measured by Fourier spectroscopy for the photon energy range of 0.008–0.8 eV and by grating spectroscopy for 0.6 –36 eV. For the measurements above 6 eV, we utilized synchrotron radiation at the Institute for Solid State Physics, University of Tokyo (INS-SOR). Measurements with changing temperature (10-290 K) were carried out between 0.008 –1.0 eV. Optical conductivity [$\sigma(\omega)$] was obtained by Kramers-Kronig analysis of the reflectivity spectra at the respective temperatures. Here, the respective spectra were combined with the room-temperature data in the higher-energy region (≥ 1.0 eV), which was confirmed to be almost temperature independent, and constant reflectivity below 0.008 eV and ω^{-4} type extrapolation above 36 eV were assumed for the Kramers-Kronig analysis. Below 0.008 eV for the metallic spectra, we attempted another type extrapolation, e.g., Hagen-Rubens type, but the deduced conductivity spectra did not show appreciable difference for an energy region above 0.02 eV.

III. STRUCTURAL TRANSITION DUE TO CHARGE ORDERING

Recently, the TEM has been proved to be a powerful probe for the CO phenomena in many TMOs.[6,8,15] More lately, we have successfully probed the existence of the CO
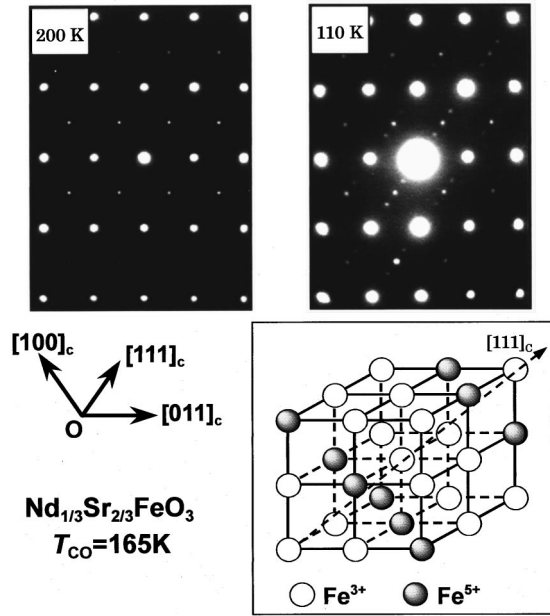
FIG. 2. $[01\bar{1}]$ zone-axis electron diffraction patterns for $Nd_{1/3}Sr_{2/3}FeO_3$ observed at 200 K and 110 K. The superlattice reflections appear along the pseudocubic $[111]_c$ direction with the modulation vector of $a_p^*=(\frac{1}{3}, \frac{1}{3}, \frac{1}{3})$.
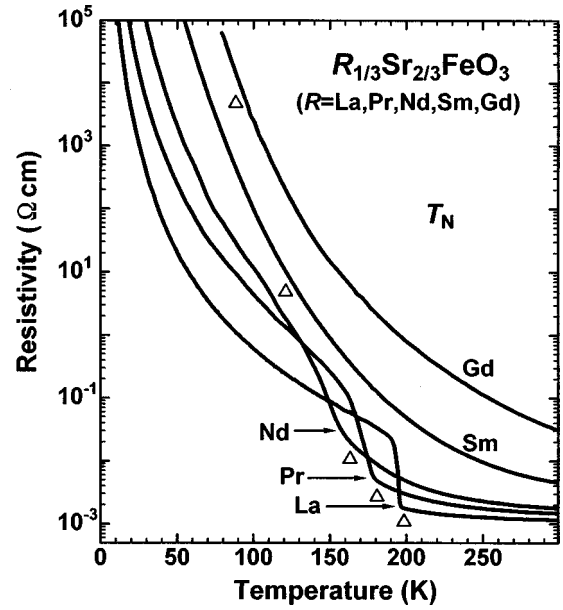

FIG. 3. Temperature dependence of resistivity for $R_{1/3}Sr_{2/3}FeO_3$ system in a cooling process. Open triangles indicate the critical temperature (T_N) for the antiferromagnetic phase transition. The T_N for $R=La$, Pr, and Nd coincides with the transition temperature (T_{CO}) for the charge ordering.

phenomena in the hole-doped $La_{1-x}Sr_xFeO_3$ $(0 \leqslant x \leqslant 0.7)$ around $x=2/3$ by means of TEM.[13] In the present paper, we have carried out TEM measurements on a series of $R_{1/3}Sr_{2/3}FeO_3$ $(R=La$, Pr, Nd, Sm, and Gd) crystals at low temperatures in order to confirm whether the CO state exists or not in the respective crystals. We exemplify in Fig. 2 the electron diffraction patterns to $[01\bar{1}]$ zone axis for the case of $R=Nd$ at 200 and 110 K, and indicate the reciprocal lattice vectors in the simple cubic setting. With decreasing temperature below 200 K, a series of sharp superstructural reflections show up along the $[111]_c$ direction in addition to the Bragg diffraction spots, as also confirmed previously for the case of the $R=La$.[13] The superlattice reflections ($\pm\frac{1}{3}$, $\pm\frac{1}{3}$, $\pm\frac{1}{3}$) indicate atomic displacements induced by CO: Nominal Fe^{3+} and Fe^{5+} species show the real-space ordering along the pseudocubic perovskite $[111]_c$ direction with a sequence of $...533533...$ (see the inset to Fig. 2), perhaps accompanying the periodic breathing-type distortion of FeO_6 octahedra. Essentially identical superlattice patterns were observed not only for $R=La$ but also for $R=Pr$, in addition to the present $R=Nd$ case. Importantly, however, such superstructural spots do not show up for $R=Sm$ and Gd down to the lowest temperature for the TEM measurement (≈ 20 K). From this, it is anticipated that the $R=Sm$ and Gd compounds do not undergo the CO transition in contrast with the larger-R $(=La$, Pr, and Nd) compounds. Such presence or absence of the CO transition depending on R species has been more firmly confirmed by spectroscopic measurements, as will be described in Sec. V.

IV. ELECTRICAL AND MAGNETIC PROPERTIES

We show in Fig. 3 temperature dependence of resistivity for crystals of $R_{1/3}Sr_{2/3}FeO_3$ $(R=La$, Pr, Nd, Sm, and Gd).

We begin with the argument on the resistivity features for the $R=La$, Pr, and Nd compounds, which undergo the CO transition. Their resistivity-values at room temperature are relatively low ($\sim 10^{-3}$ Ω cm) and slightly increase with decreasing ionic radius of the R site (or with a decrease of W). When temperature is decreased, the resistivity shows gradual semiconductorlike increase down to T_{CO}, and then undergoes a sudden change upon the CO transition, followed by a steep increase below T_{CO}. On the other hand, for the $R=Sm$ or Gd compounds with smaller W, in which CO is not observed in the TEM, the resistivity shows an insulating feature without any distinct anomaly or jump over the whole temperature region. In the low-temperature region these resistivity (ρ) data can be described well by variable range hopping (VRH)-type formula[16,17] $[\ln \rho(T) \propto T^{-1/4}]$ rather than the activation type $[\ln \rho(T) \propto T^{-1}]$, in particular for the $R=Sm$ and Gd compounds showing no CO transition. The VRH model represents a tunneling conduction between the orbitals in the presence of random potential. Presumaly Coulomb disorder due to the (R, Sr) substitution is a likely origin of VRH for such a near-localized state in the antiferromagnetic phase *(vise versa)*. Incidentally, the resistivity of $LaFeO_3$ $(x=0)$, and perhaps of other $RFeO_3$ $(x=0)$, is typically insulating, $>10^6$ Ω cm below room temperature, due to the large charge gap (~ 2 eV).[9] The remarkably R-dependent features of resistivity are summarized as follows: (1) The resistivity increases from $R=La$ to Gd with a decrease of W due to increasing lattice distortion. (2) The resistivity for $R=La$, Pr, and Nd shows an abrupt increase at T_{CO} due to the CO transition, which is of the first order with a thermal hysteresis of ~ 3 K in width. (3) With increasing lattice distortion in going from La to Nd, the CO state becomes unstable: T_{CO} shifts to lower temperature, and the resistivity jump at T_{CO} becomes blurred. In the case of $R=Sm$ and Gd with larger lattice distortion, the resistivity
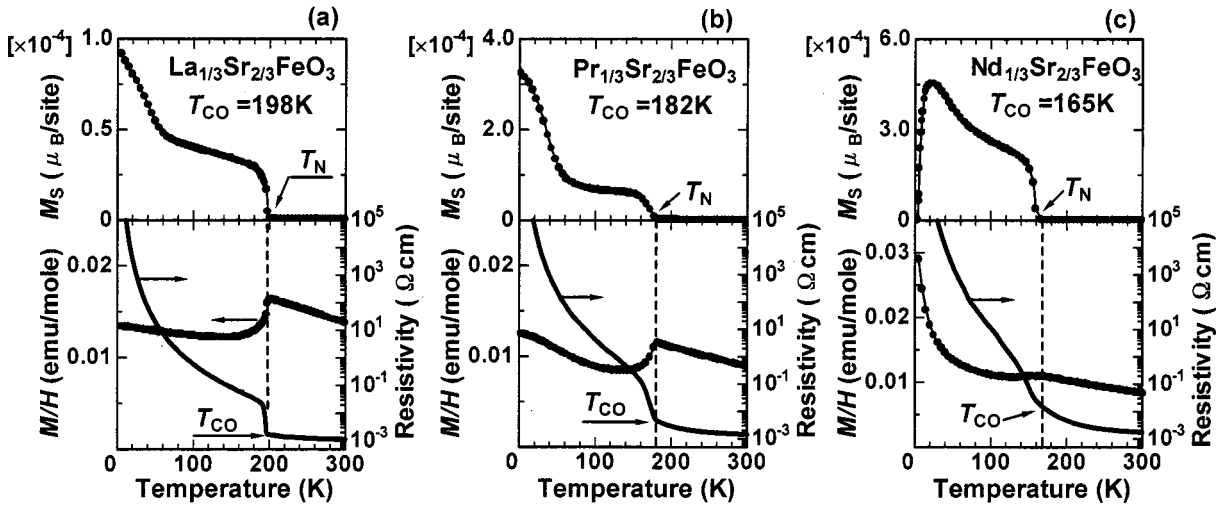
FIG. 4. Correlation between the temperature dependencies of resistivity (lower panels), magnetization M at $\mu_0 H = 1$ T (lower panels) and spontaneous magnetization M_s (upper panels) for $R_{1/3}Sr_{2/3}FeO_3$ systems, (a) R=La, (b) Pr, and (c) Nd, all of which undergo the CO transition accompanying with the antiferromagnetic spin ordering ($T_{CO} = T_N$).

jumps as a signal of the CO transition no longer shows up while the resistivity shows VRH-type insulating behavior over the whole temperature range.

The CO transitions in TMO's show up occasionally accompanied by the antiferromagnetic spin ordering as well as by the concomitant lattice distortion.[1] The present $R_{1/3}Sr_{2/3}FeO_3$ system is also the case. We show in Figs. 4(a)–4(c) the temperature dependence of the magnetization and resistivity (lower panels) together with the spontaneous magnetization (upper panels) for R=La, Pr, and Nd, which undergo the CO transition. The corresponding results for R=Sm and Gd are shown in Figs. 5(a) and 5(b), respectively. We could deduce the magnetic ordering temperature (T_N: Nèel temperature) from the onset of the tiny spontaneous magnetization (M_s) at 0 T, which arises from minute spin canting in the antiferromagnetically ordered state in the slightly distorted perovskite structure (see the upper panels of Figs. 4 and 5). In the case of R=La, Pr, and Nd (i.e., the CO system), the magnetization (M/H) at a higher magnetic field (1 T) shows a clear cusp structure characteristic of the
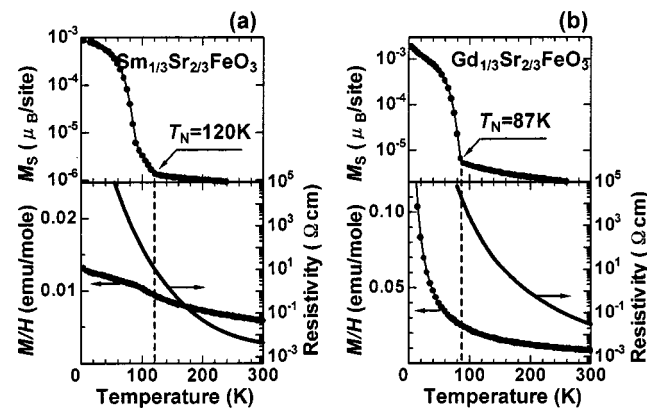
FIG. 5. Correlation between the temperature dependencies of resistivity, magnetization, and spontaneous magnetization for (a) R=Sm and (b) Gd which do not undergo the CO transition, although the spin ordering occurs below T_N. The measurement condition was the same as in Fig. 4.

antiferromagnetic transition, at which the resistivity shows abrupt increase. Thus, these systems undergo the phase change from a paramagnetic metallic state to an antiferromagnetic charge-ordered state at T_{CO} ($= T_N$). The charge-ordered state has in fact been assigned to the ordering of magnetically different Fe sites composed of the nominal Fe^{3+} ($3d^5$) and Fe^{5+} ($3d^3$) sites with the ratio of 2:1 (Refs. 11–13). However, in the case of R=Sm and Gd (see Fig. 5), the cusp structure in the M–T curve is weak (R=Sm) or nearly vanishes (R=Gd) and no distinct change of the resistivity is observed around T_N. This confirms again that there occurs no CO transition for R=Sm and Gd.

Looking at Figs. 4 and 5, one may notice that the T_N is shifted to lower temperature by increasing lattice distortion (with decrease of the W). This is perhaps because the magnitude (J_{AF}) of an antiferromagnetic interaction between the Fe spins is reduced due to decrease of the W (or the p-d hybridization). Furthermore, the decrease of the J_{AF} appears also to destabilize the CO phase, since the antiferromagnetic spin ordering in the present system always shows up concomitantly with the CO transition ($T_N = T_{CO}$). The T_{CO} is shifted to a lower temperature together with decrease of the T_N (see also Fig. 8) and finally disappears with further decreasing J_{AF} (for R=Sm and Gd) while T_N remains around 100 K.

V. OPTICAL SPECTROSCOPY

To argue the effect of the CO transition on the electronic structure and lattice dynamics, we have previously investigated the temperature dependence of the optical reflectivity spectra for the R=La compound.[18] In this paper, a systematic study of optical spectra has been extended to a whole series of $R_{1/3}Sr_{2/3}FeO_3$ (R=La, Pr, Nd, Sm, and Gd) to probe the CO transition in terms of changes in lattice dynamics as well as optical-gap structures in a low-energy region ($\leqslant 1.0$ eV).

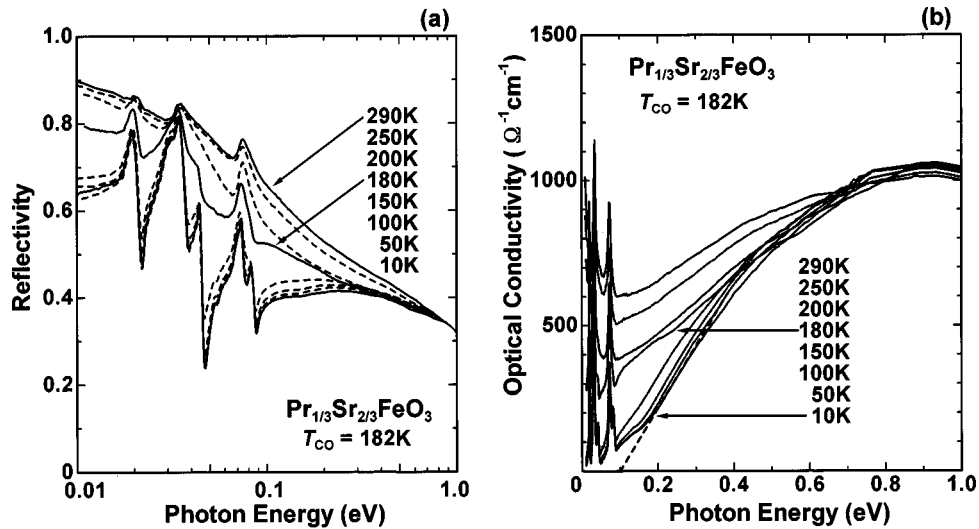We show in Fig. 6(a) the temperature dependence of the reflectivity spectra below 1.0 eV for the R=Pr, as a repre-

FIG. 6. Temperature dependence of (a) the reflectivity spectra and (b) the optical conductivity spectra below 1 eV for $Pr_{1/3}Sr_{2/3}FeO_3$. A dashed line in (b) is extrapolation of the onset part of the 0.9 eV-peak for the estimate of the optical gap energy at 10 K.

sentative example for the CO transition system. The reflectivity below 1.0 eV steeply increases toward 1 with lowering photon energy at temperatures above T_{CO} (182 K), reflecting the metallic value of resistivity ($\sim 10^{-3}$ Ω cm). Once the temperature is decreased below T_{CO}, the reflectivity is abruptly suppressed and the shape of the spectrum shows an insulating feature. Spiky structures below 0.1 eV are due to the optical phonon modes, the number of which is clearly increased after the system undergoes the CO transition.

The electronic-structural change upon the CO transition is more clearly visible in the optical conductivity [$\sigma(\omega)$] spectra shown in Fig. 6 (b), which were derived by the aforementioned Kramers-Kronig transformation of the reflectivity spectra. The conductivity value obtained by the zero-frequency extrapolation of the spectrum is in accord with the dc conductivity value, suggesting that the electronic structure in this energy region must dominate charge transport as well. Above T_{CO}, a Drude component, namely a sharply increasing component toward $\omega = 0$, is observed below 0.1 eV, signaling the existence of the carriers in coherent motion corresponding to a metallic value of the resistivity. The Drude weight below 0.1 eV is decreased with decreasing temperature. Once the system undergoes the CO transition by further decreasing temperature, the spectral weight below 0.7 eV decreases significantly, resulting in the opening of an optical gap. The broad conductivity maximum around 0.9 eV can be assigned to charge-transfer-type transitions between O $2p$ and Fe^{4+} e_g states with the final states of $t_{2g\uparrow}^3 e_{g\uparrow}^2$ as in the case of $R = La$.[18]

Figure 7 compares the ground-state (10 K) spectra of optical conductivity for all the $R_{1/3}Sr_{2/3}FeO_3$ ($R = La$, Pr, Nd, Sm, and Gd) compounds, which all show the gaplike feature. We attempted to estimate the magnitude of the optical gap energy in the ground state by extrapolating the onset part linearly to the base line of the $\sigma(\omega) = 0$, as exemplified by a dashed line for the 10 K spectrum for the $R = Pr$ compound shown in Fig. 6(b). Due to the blurred feature of the onset part of the spectra, it is not straightforward to accurately estimate the optical gap (2Δ), but the crosspoint may give a

crude measure for 2Δ. We show in the bottom panel of Fig. 8 the R-dependence of 2Δ. The value of 2Δ gradually increases with increasing lattice distortion. This may be ascribed to the increase of the effective intersite Coulomb repulsion due to the decrease in the hopping interaction, since the optical gap has a character of the interatomic d-d transition. As exemplified for $R = Nd$ in Fig. 6(b), the gap observed for the charge-ordered ground state of $R = La$, Pr, and Nd disappears or tends to zero with increaseing temperature above T_{co}. Likewise, the real-gap feature for the non-CO ($R = Sm$ and Gd) compounds at the ground state arises from the antiferromagnetic spin ordering. However, the reduced p-d hybridization of these non-CO systems already gives rise to a gaplike feature in the $\sigma(\omega)$ spectra even above the antiferromagnetic transition temperature (T_N), as typically seen in the reduced low-energy ($\gtrsim 0.1$ eV) spectral weight
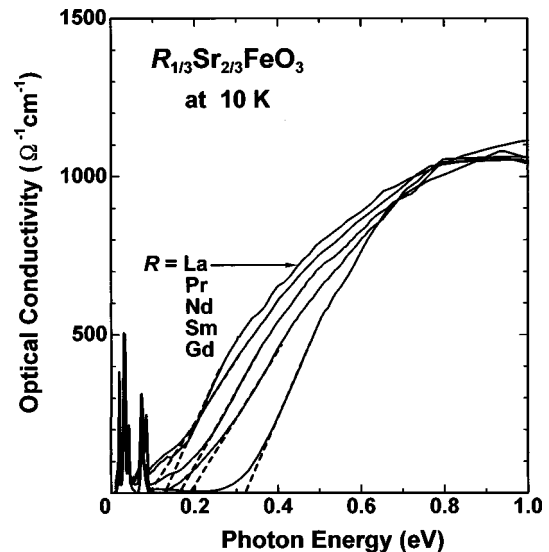

FIG. 7. Optical conductivity spectra at 10 K (viewed as representing the ground state) for $R_{1/3}Sr_{2/3}FeO_3$ ($R = La$–Gd). Dashed lines are extrapolations of the onset parts for the estimate of the respective optical gaps.
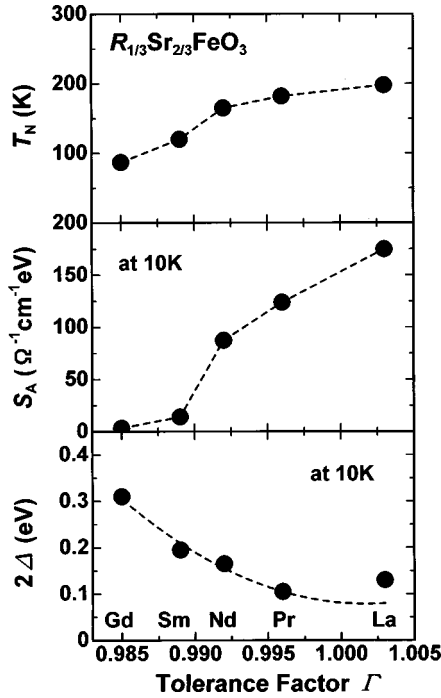
FIG. 8. R dependence of various physical quantities for the $R_{1/3}Sr_{2/3}FeO_3$ (R=La–Gd) system. The top panel: the critical temperatures (T_N) for the antiferromagnetic phase transition; the middle panel: the oscillator strength (S_A) of the activated optical phonon mode at 10 K (see also the caption of Fig. 10); the bottom panel: the optical gap (2Δ) (see Fig. 7 and text).

(apart from the optical phonon peaks); see in the lower panel (for R=Sm and Gd) of Fig. 9.

Next, to argue the possible lattice-structural change upon the CO transition, we show in Fig. 9 the $\sigma(\omega)$ spectra in a lower-energy region below 0.1 eV for R=Pr–Gd. As demonstrated for the case of R=La,[18] the infrared phonon spectra can furnish a conclusive evidence of the CO transition accompanied by the lattice distortion: The optical phonon modes in the CO state are split due to the folding of the phonon dispersion branch caused by the periodic lattice distortion. All the samples show sharp peak structures in the optical conductivity spectra at room temperature due to the optical phonon modes, the number of which is consistent with the expectation for the cubic perovskite structure; namely the external mode around 0.02 eV, the bending mode around 0.033 eV, and stretching mode around 0.073 eV, respectively. Although all the samples have rhombohedral symmetry slightly distorted from a cubic perovskite structure at room temperature, the rhombohedral distortion is too small for any activated phonon modes to be discerned. Once the temperature decreases below T_{CO}, the bending and stretching modes are subject to the large spectral change, shift and splitting, for R=Pr and Nd, as seen in Fig. 9. In fact these modes are more sensitive to the Fe-O bond distortion than the external mode. The breathing type distortion of FeO$_6$ octahedra may occur on the nominal Fe^{5+} site in the CO state to acquire the energy gain due to the crystal field or p-d hybridization. By contrast, the R=Sm and Gd compounds show merely a small spectral change for the bending modes and essentially no spectral change for the stretching modes. Such a R-dependent temperature variation of optical
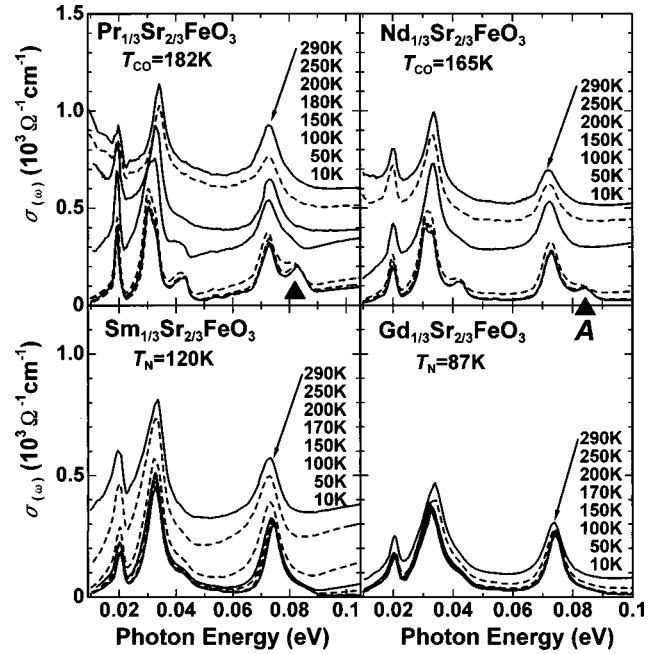

FIG. 9. Temperature dependence of the optical conductivity spectra in the optical phonon region below 0.1 eV for the $R_{1/3}Sr_{2/3}FeO_3$ (R=Pr–Gd) system. Filled triangles indicate the new optical phonon mode (referred to as the A peak) of the Fe-O stretching which is utilized for estimate of the CO-induced lattice deformation.

phonon modes confirms again the presence (for R=La, Pr, and Nd) and the absence (for R=Sm and Gd) of the CO transition.

We utilize the spectral intensity of the activated mode at 0.083 eV (indicated by closed triangles and referred to as the A peak in Fig. 9) as a measure of the CO order parameter. The A peak is due to folding of branches of the Fe-O stretching mode by the periodic charge modulation and/or associated lattice distortion along the $[111]_c$ direction in the CO state. The oscillator strength of the A peak should reflect the magnitude of the Fe-O bond distortion arising from the charge modulation. Such an activated-phonon spectral intensity is highly sensitive also to short-range or dynamical CO, reflecting the local and high-frequency nature of this probe. We have estimated the oscillator strength of the A peak by the conventional Drude and Lorentz curve fitting analysis with use of the following formula:

$$\sigma(\omega) = \frac{\sigma_0}{1+(\omega\tau_0)^2} + \sum_{j=1}^{k} \frac{S_j \omega_j^2 \gamma_j \omega^2}{(\omega_j^2 - \omega^2)^2 + \gamma_j^2 \omega^2}. \quad (2)$$

Here, σ_0 represents the dc conductivity, τ_0 and $1/\gamma_j$ represent lifetime, and ω_j and S_j are phonon frequency and oscillator strength, respectively. For the fitting, we assumed k=4 above T_{CO} and k=8 below T_{CO} in the cases of the R =Pr and Nd, or below 200 K for R=Sm and Gd. We show in Fig. 10 the temperature dependence of the oscillator strength (S_A) in the A peak for all the samples. (The data for R=La are quoted from our previous result in Ref. 18.) The value of S_A steeply increases across T_{CO}, and is nearly saturated below 130 K for the CO systems with R=La, Pr, and Nd. It is worth noting that the value of the S_A, e.g., at the
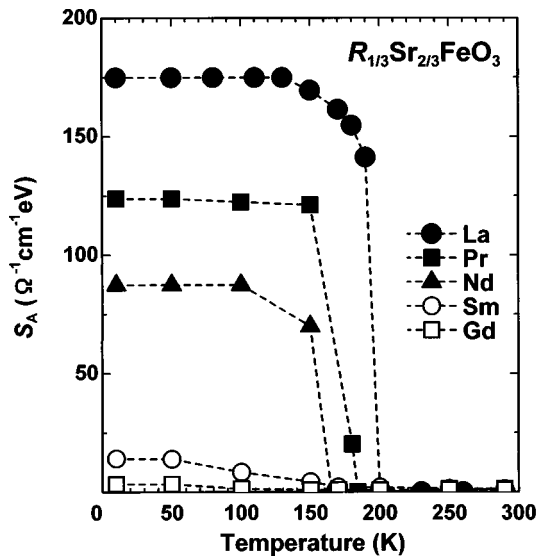
FIG. 10. Temperature dependence of the oscillator strength (S_A) of the activated A peak (see the caption of Fig. 9) for the $R_{1/3}Sr_{2/3}FeO_3$ ($R=$La–Gd) system. Dashed lines are merely the guides to the eyes.

lowest temperature (10 K), decreases systematically with decreasing the R-ion size from La to Nd (see also the middle panel of Fig. 8), indicating the decrease of the CO order parameter in this order. The discontinuous increase of S_A at T_{CO} for $R=$La, Pr, and Nd indicates that the CO transition is the first-order phase transition. The $R=$Sm and Gd compounds show a minimal value of S_A over the whole temperature region, in accord with the absence of the CO transition in these compounds. The tiny signal intensity for $R=$Sm may imply the dynamical or short-range CO correlation left in this compound.

VI. CONCLUSION

We have investigated transport, magnetic, and optical properties relevant to the CO transition for melt-grown crystals of $R_{1/3}Sr_{2/3}FeO_3$, where $R=$La, Pr, Nd, Sm, and Gd. A decrease in the ionic radius of the R site by changing R from La to Gd increases a rhombohedral lattice distortion in this system, which leads to decrease in hybridization between O $2p$ and Fe $3d$ states or the one-electron bandwidth (W). There are observed several remarkable R-dependent features: With change of R from La to Gd, (1) the resistivity at room temperature gradually increases due to decrease in W (see Figs. 4 and 5); (2) the Nèel and charge-ordering (CO) temperatures, T_N and T_{CO}, are shifted to lower temperature, and for $R=$Sm and Gd no CO transition takes place while T_N remains around 100 K (see the top panel of Fig. 8). (3) A clear gap opening due to the CO transition is observed in the optical conductivity spectra for $R=$La, Pr, and Nd, while the gap energy (2Δ) in the ground state gradually increases by a decrease of the W irrespective of the presence or absence of the CO (see the middle panel of Fig. 8). (4) New optical phonon modes are activated, or the original modes are split due to the charge modulation and associated breathing-type lattice distortion along $[111]_c$. With decreasing temperature across T_{CO}, the oscillator strength for the activated mode steeply increases in the cases of $R=$La, Pr, and Nd, while for $R=$Sm and Gd the corresponding modes remain almost silent over a whole temperature region (see Fig. 10).

All these results indicate that the CO instability is rather decreased with decrease of the R-site ionic radius or decrease of the p-d hybridization effect. This is apparently in contradiction with the intuition that the reduced bandwidth may favor the charge-ordered state. However, we may have to consider the unusual valence state of nominal Fe^{5+} involved in the charge-ordered state of the present compounds. Such a high-valence state with $S=3/2$ is obviously stabilized not only via the coupling with the breathingtype distortion, but also via the strong p-d hybridization endowing the Fe^{5+} site with dominant p-hole character.

*Present address: Central Research Laboratory, Hitachi Ltd., Kokubunji, Tokyo 185-8601, Japan.

†Present address: Department of Applied Physics, Tokyo Institute of Technology, Oh-okayama, Tokyo 152-8551, Japan.

‡Present address: National Laboratory for Superconductivity, Institute of Physics & Center for Condensed Matter Physics, Chinese Academy of Sciences, Beijing 100080, China.

[1] For a review, see M. Imada, A. Fujimori, and Y. Tokura, Rev. Mod. Phys. **70**, 1039 (1998).

[2] E. J. Verwey and P. W. Haayman, Physica (Amsterdam) **8**, 979 (1941).

[3] J. M. Tranquada, B. J. Sternlieb, J. D. Axe, Y. Nakamura, and S. Uchida, Nature (London) **375**, 561 (1995).

[4] Z. Jirak, S. Krupicka, Z. Simsa, M. Dlouha, and Z. Vratislav, J. Magn. Magn. Mater. **53**, 153 (1985).

[5] H. Kuwahara, Y. Tomioka, A. Asamitsu, Y. Moritomo, and Y. Tokura, Science **270**, 961 (1995).

[6] C. H. Chen, S.-W. Cheong, and A. S. Cooper, Phys. Rev. Lett. **71**, 2461 (1993).

[7] S.-W. Cheong, H. Y. Hwang, C. H. Chen, B. Batlogg, L. W. Rupp, Jr., and S. A. Carter, Phys. Rev. B **49**, 7088 (1994).

[8] Y. Moritomo, Y. Tomioka, A. Asamitsu, Y. Tokura, and Y. Matsui, Phys. Rev. B **51**, 3297 (1995).

[9] T. Arima, Y. Tokura, and J. B. Torrance, Phys. Rev. B **48**, 17 006 (1993).

[10] S. K. Park, S. Yamaguchi, and Y. Tokura (unpublished).

[11] M. Takano and Y. Takeda, Bull. Inst. Chem. Res., Kyoto Univ. **61**, 406 (1983).

[12] P. D. Battle, T. C. Gibb, and P. Lightfoot, J. Solid State Chem. **84**, 271 (1990).

[13] J. Q. Li, Y. Matsui, S. K. Park, and Y. Tokura, Phys. Rev. Lett. **79**, 297 (1997).

[14] R. D. Shannon, Acta Crystallogr., Sect. A: Cryst. Phys., Diffr., Theor. Gen. Crystallogr. **32**, 751 (1976).

[15] J. Q. Li, Y. Matsui, T. Kimura, and Y. Tokura, Phys. Rev. B **57**, R3205 (1998).

[16] N. F. Mott, Philos. Mag. **19**, 835 (1969).

[17] R. H. Wallis, N. Sol, and A. Zylbersztejn, Solid State Commun. **23**, 539 (1977).

[18] T. Ishikawa, S. K. Park, T. Katsufuji, T. Arima, and Y. Tokura, Phys. Rev. B **58**, R13 326 (1998).